RESEARCH ARTICLE

Gestational Hypoxia Induces White Matter Damage in Neonatal Rats: A New Model of Periventricular Leukomalacia

Olivier Baud[1]; Jean-Luc Daire[2]; Yvette Dalmaz[3]; Romain H. Fontaine[1]; Richard C. Krueger[4]; Guy Sebag[2]; Philippe Evrard[1]; Pierre Gressens[1]; Catherine Verney[1]

[1]Laboratoire de Neurobiologie du Développement, INSERM E9935, Service de Néonatologie et Service de Neurologie, Hôpital Robert Debré, Paris, France.
[2]Service d'imagerie médicale, Hôpital Robert Debré, Paris, France.
[3]Laboratoire de Physiologie des Régulations Energétiques, Cellulaires et Moléculaires, UMR CNRS 5123, Lyon, France.
[4]Division of Neonatology, Cedars Sinai Medical Center, Los Angeles, Calif.

Corresponding author:
Catherine Verney, PhD, INSERM E9935, Hôpital Robert Debré, 48 bd Sérurier 75019 Paris, France (E-mail: cverney@infobiogen.fr)

In the premature infant, periventricular leukomalacia, usually related to hypoxic-ischemic white matter damage, is the main cause of neurological impairment. We hypothesized that protracted prenatal hypoxia might induce white matter damage during the perinatal period. Pregnant Sprague-Dawley rats were placed in a chamber supplied with hypoxic gas (10% O_2-90% N_2) from embryonic day 5 (E5) to E20. Neonatal rat brains were investigated by histology, immunocytochemistry, western blotting, in situ hybridization, DNA fragmentation analysis, and in vivo magnetic resonance imaging (MRI).

Body weight of pups subjected to prenatal hypoxia was 10 to 30% lower from P0 to P14 than in controls. Specific white matter cysts were detected between P0 and P7 in pups subjected to prenatal hypoxia, in addition to abnormal extra-cellular matrix, increased lipid peroxidation, white matter cell death detected by TUNEL, and increased activated macrophage counts in white matter. Subsequently, gliotic scars and delayed myelination primarily involving immature oligodendrocytes were seen. In vivo MRI with T1, T2, and diffusion sequences disclosed similar findings immediately after birth, showing strong correlations with histological abnormalities. We speculate that protracted prenatal hypoxia in rat induces white matter damage occurring through local inflammatory response and oxidative stress linked to re-oxygenation during the perinatal period.

Brain Pathol 2004;14:1-10.

INTRODUCTION

The normal development and maturation of the central nervous system may be affected by various environmental factors, either prenatally or perinatally (20). Hypoxia may be prominent among these factors. Hypoxia occurs in association with many abnormal conditions including reduced uteroplacental blood flow (secondary to maternal hypertension, smoking, or use of alcohol or cocaine), constitutive abnormal placental function, high altitude, maternal anemia, or acute maternal hypoxia. Fetal hypoxia secondary to uteroplacental vascular disease carries a risk of intrauterine growth retardation, respiratory disease, and neural disorders including cerebral palsy (12, 20, 22, 33).

Cerebral palsy in infants born prematurely is strongly associated with white matter damage, most notably periventricular leukomalacia (14). Although the cause of the white matter lesions remains incompletely understood, clinical and experimental data suggest a major pathophysiological role for inflammation and/or oxidative stress (8). In several animal models, white matter damage is obtained by inducing either a systemic inflammatory response or hypoxia-ischemia (8). Other models involve activation of NMDA and non-NMDA glutamate receptors and point to excitotoxicity as a causative factor in white matter injury (6, 8, 17). To our knowledge, whether pure oxygen deprivation during pregnancy directly affects the developing white matter has not been evaluated.

We hypothesized that protracted prenatal hypoxia might induce white matter lesions during the perinatal period and that oxidative stress related to re-oxygenation immediately before birth might participate in the pathophysiology of these lesions. We examined this hypothesis in rats by subjecting pregnant females to hypoxia and examining the neonatal brains by histology, immunocytochemistry, western blotting, in situ hybridization, DNA fragmentation analysis, and in vivo magnetic resonance imaging (MRI). The results show that protracted prenatal hypoxia in rats is a model of white matter damage related to both oxidative stress and a local inflammatory response.

METHODS

Animal model of long-term gestational hypoxia in rat. Pregnant rats (Sprague-Dawley, Charles River Laboratory, L'Arbresle, France) were placed from embryonic day (E)5 to E19 (E0 being the day of mating) in a normobaric Plexiglas chamber supplied with a gas mixture that either induced hypoxia (10% O_2-90% N_2 with O_2 kept at 10 ± 0.5%) or maintained normoxia (21% O_2-79% N_2 with O_2 kept at 21 ± 0.5%), as described by Peyronnet et al (23). Expired CO_2 in the chamber was consistently less than 0.1%, and the temperature inside the chamber was set at 26 ± 1°C. On the day before delivery (E20), the dams were removed from the chamber and housed individually under normoxic conditions. After delivery, 15 to 35 hypoxic and normoxic pups were studied at each of the following postnatal (P) ages: P0 (day of birth), P3, P7, P14, and P21; in all, 156 normoxic and 115 hypoxic pups were examined. For western blotting analysis the brains were dissected separating the cerebral wall from the ventral telencephalic -diencephalic regions. In addition, prenatal E19 fetuses were obtained under anesthesia (chloral hydrate, 350 mg/kg) from three

NAME	MANUFACTURER	TYPE	DILUTION
GLUT1	Biogenesis, Sandown, NH	Rabbit polyclonal	1:500
GFAP	Sigma, St Louis, Mo	Mouse monoclonal	1:500
S100β	Swant, Bellinzona, Switzerland	Rabbit polyclonal	1:2000
OX42	Serotec, Raleigh, NC	Mouse monoclonal	1:250
Tomato lectin	Vector, Burlingame, Calif	Biotin conjugated	1:200
O4	Generous gift from Dr P Rosenberg	Mouse monoclonal	1:500
MBP	Sigma, St Louis, Mo	Mouse monoclonal	1:1000
RT97	Roche, Meylan, France	Mouse monoclonal	1:1000
PSA-NCAM	Generous gift from Dr G Rougeon	Mouse monoclonal	1:5000
Reduced HNE	Calbiochem, San Diego, Calif	Rabbit polyclonal	1:100

Table 1. Primary antibodies used in this study: axonal marker (neurofilament RT97); astrocyte markers (glial fibrillary acidic protein [GFAP] and protein Sβ100 [S100β]); oligodendrocyte markers (O4, myelin basic protein [MBP]); microglial cell markers (OX42, tomato lectin); extracellular matrix marker (polysialylated NCAM [PSA-NCAM]); lipid peroxidation marker (reduced HNE); and vascular endothelial cell marker (GLUT1).

normoxic dams (17 fetuses) and 4 hypoxic dams (31 fetuses). All experimental protocols complied with the guidelines issued by the Institut National de la Santé et de la Recherche Médicale (INSERM) and with the EU Council Directives for the care of laboratory animals (No. 02889).

Metabolic measurements. Blood samples (400 μl) were drawn from the tail vein of normoxic and hypoxic dams on gestational day 19, into microtubes containing 795 μl of 1 M perchloric acid for deproteination and 5 μl heparin. After centrifugation (5000g for 15 minutes), the plasma was collected, aliquoted, and kept at -80°C. Lactate, pyruvate, and ketone bodies (beta-hydroxy-butyrate and aceto-acetate) were measured enzymatically as previously described by Vassault et al (29).

Immunocytochemistry. At each studied postnatal stage (P0, P3, P7, P10, P14 and P21), 4 to 6 pups in each group were anesthetized with isoflurane and transcardially perfused with 4% paraformaldehyde in phosphate buffer (PB 0.12 M, pH 7.4). After rinses in 10% sucrose in PB, the cryoprotected brains were frozen in liquid nitrogen-cooled isopentane and stored at -80°C. The brains were cut into serial 10-μm thick cryostat sections, which were alternately processed for immunocytochemistry or Nissl staining. The primary antibodies were directed against various antigens specific of cell types (microglia, astrocytes and neurons) or cytoarchitectonic markers (Table 1). The sections were rinsed in 0.25% PBS/Triton X-100/0.2% gelatin (PBS-TX-gel) and incubated overnight at room temperature with appropriately diluted primary antibody in PBS-TX-gel with 0.02% sodium azide. The primary antibodies were visualized after incubations with the appropriate species-specific biotinylated secondary antibody (Table 1) and the streptavidin-biotin-peroxidase complex (3). For *Lycopersicon esculentum* (tomato) lectin (Vector Laboratories, Burlingame, Calif), the streptavidin-biotin-peroxidase method was used without secondary antibody.

For immunofluorescence double staining, sections were incubated overnight with a mixture of 2 primary antibodies in concentrations of twice the dilutions shown in Table 1. The second incubation was performed with a secondary antibody conjugated either with Texas red (1:200, Vector, Burlingame, Calif) labeling in red or with fluorescein-isothiocyanate (FITC, 1:50, Sigma, St Louis, Mo) labeling in green (GFAP). Controls obtained by omitting the primary antibody were run for each immunocytochemical method.

TUNEL staining. Cell death in white matter was detected using TUNEL staining as previously described (31). On each section, labeled nuclei were counted throughout the hemispheric white matter at E19, P3, and P7 in at least 4 animals at each age and in each group (hypoxic and control). Results were expressed as means ± standard error of the mean (SEM) and compared using the nonparametric Mann-Whitney test.

Microscopy. For most counts, sections at the same coronal level of brains from the hypoxic animals and the controls included the septal area or the dorsal hippocampal formation (Paxinos, 1998 [22], Figures 15 to 20). The cingulate, motor, and somatosensory cortical areas were examined, as well as the underlying white matter including the corpus callosum and cingulum. A CDD camera (Apogee Instrument Inc., Boston, Mass) was used to digitize the region of interest in order to improve the accuracy of the labeled-cell counts. In each group (hypoxic and control), 4 to 6 animals at each developmental stage were studied; at least 3 nonadjacent fields in a section included within a square-grid reticule were examined. Vessel wall density was evaluated by counting the intersections of each labeled vessel wall with the square-grid reticule at ×10 magnification in a one mm^2 area. Cell counts were made at either ×40 or ×20 magnification in two areas, of 0.065 mm^2 and 0.25 mm^2, respectively. The observer who examined the sections was not aware of the developmental stage or group.

Results were expressed as means ± SEM. Statistical analysis of the histological data was performed using either 2-way ANOVA with a Bonferroni post-test or the Mann-Whitney test, as appropriate (PRISM software).

In situ hybridization. The aggregating proteoglycans including aggrecan are important components of many extracellular matrices (27). AmpiTaq Gold polymerase (Perkin-Elmer Inc., Boston, Mass) was used to amplify cDNAs for aggrecan and TGF-beta2, using relevant primers and template cDNA derived from mouse P1 cartilage or brain tRNA. The cDNAs were synthesized using Superscript II R (Gibco/Invitrogen, Calrsbad, Calif) and the tRNA was purified using the ToTALLY RNA kit (Ambion, Austin, Tex). A single 527-bp cDNA fragment for TGF-beta2 was amplified using the following primers: forward 5′-TTCTA TTGGG CATTA ACTTT CGACT G; and reverse 5′-GTAGG GTCTG TAGAA AGTGG GCGG). A single 513-bp cDNA fragment for aggrecan was amplified using the following primers: forward: 5′-GGTTC AGAAT TCTCT ACCTC TG-GAA TAGAG GACAT CAGTG TACT; and reverse: 5′-AAGAT CGTCG ACTCC AGAGG CAGAA GTTTC TAGAC CC). Fragments were cloned into pCRR II-TOPO (Invitrogen/Gibco) using the TA

cloning kit. Sequences were confirmed by sequencing.

Purified plasmids containing either the TGF-beta2 or the aggrecan fragment were cleaved by XhoII and PvuII. The 832-bp or 846-bp restriction fragments thus obtained were gel purified; these fragments containing the PCR fragments under the control of an SP6 promoter were used to synthesize an antisense riboprobe.

Digoxigenin-labeled antisense RNA probes were synthesized using SP6 RNA polymerase (Roche, Meylan, France) and purified using the Megapure kit (Ambion). Purified probes were analyzed for homogeneity by electrophoresis and quantified by dot blot.

In situ hybridization was performed on brains harvested after decapitation and immediately frozen in liquid nitrogen. Cryostat sections 15 µm in thickness were dried at room temperature and postfixed in paraformaldehyde 4% for 20 minutes. Prehybridization was performed in buffer containing salmon sperm DNA and Denhardt's 1×. The slides were incubated with 200 ng/ml of each antisense RNA denatured digoxigenin-labeled probe, at 62°C for 20 hours. After several washes, endogenous phosphatase was blocked with 2% blocking reagent (Roche) before incubation overnight at room temperature with an anti-digoxigenin antibody conjugated to alkaline phosphatase (1:2000, Roche). The specific digoxigenin-labeled probe was detected using nitroblue tetrazolium and 5-bromo-4-chloro-3-indolyl phosphate toluidonium salt as the substrates.

Western blot. Briefly, for Western blot analysis, protein extracts from the cerebral wall or ventral telencephalon-diencephalon were separated by electrophoresis in 10% polyacrylamide gel, transferred to a nitrocellulose membrane, and immunoreacted with reduced-HNE-protein antibody (Table 1). Nitrocellulose was further processed using horseradish peroxidase (HRP)-conjugated anti-rabbit secondary antibody (1:5000, Chemicon, Temecula, Calif) and a chemiluminescent system (PerkinElmer). Major bands thus visualized were quantitated using Quantity One software (Biorad, Hercules, Calif).

In vivo magnetic resonance imaging (MRI). *MRI acquisition*. MRI was performed using a 1.5 Tesla machine (Philips Intera, Best, The Netherlands) with a circular surface microscopic coil (diameter, 2 cm). For all animals (P0: n = 12; P7: n = 14), three sequences were used: T2-weighted Turbo Spin Echo; T1-weighted Inversion Recovery with an inversion time (TI) of 900 ms; and the diffusion-weighted spin-echo echo-planar-imaging (SE-EPI) sequence with three b values (0, 300 and 600 sec/mm^2) for the diffusion gradients. The voxel size was 250 µm × 250 µm × one mm for T1- and T2-weighted sequences and 300 µm × 300 µm × one mm for diffusion imaging. Images were acquired in a coronal plane identical to the plane used for the histological sections. Eight slices were acquired in the coronal plane using all three sequences, with identical geometric parameters for orientation and position.

The rats were restrained in a nontraumatic flexible holder without anesthesia. No clinical evidence of discomfort or impaired alertness was noted. Body temperature was controlled and maintained at 37°C using a

Maternal Blood Samples at E19	Normoxic (n = 10)	Hypoxic (n = 8)	p
Lactate (mmol/L)	3.36 ± 0.30	3.49 ± 0.44	0.8
Pyruvate (µmol/L)	160 ± 13	142 ± 14	0.3
Aceto-acetate (mmol/L)	28.9 ± 6.7	27.3 ± 9.8	0.9
βOH butyrate (mmol/L)	55.6 ± 13	64.3 ± 27.7	0.8

Table 2. Monocarboxylate levels in maternal serum on E19 (Mann-Whitney test).

	White Matter Inflammation	Focal White Matter Lesions	Astrogliosis	Myelination Delay
E19 (n = 10)	8 (80%)	0	nd	nd
P0 (n = 14)	14 (100%)	11 (79%)	nd	nd
P3 (n = 17)	17 (100%)	16 (94%)	0	nd
P7 (n = 15)	3 (20%)	3 (20%)	12 (67%)	17 (95%)
P14 (n = 5)	0	0	5 (100%)	5 (100%)
P21 (n = 6)	nd	0	5 (83%)	1 (17%)

Table 3. Numbers (%) of hypoxic pups with white matter damage, by age. (nd: not determined)

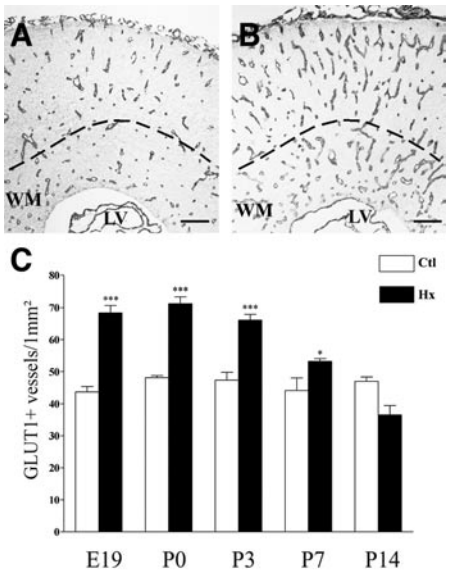

Figure 1. Coronal sections showing GLUT1 immunostaining on E19 in the cerebral cortex and white matter (WM) in control (**A**) and hypoxic (**B**) pups. LV: lateral ventricle. The red line separates the cortex from the underlying white matter. Bar = 30 µm. **C.** Quantitative analysis of vessel wall density in white matter according to age. The bars represent the mean ± SEM. The asterisks indicate significant differences between controls and hypoxic groups (***p<0.001 and *p<0.05 in 2-way ANOVA with the Bonferroni comparison post test).

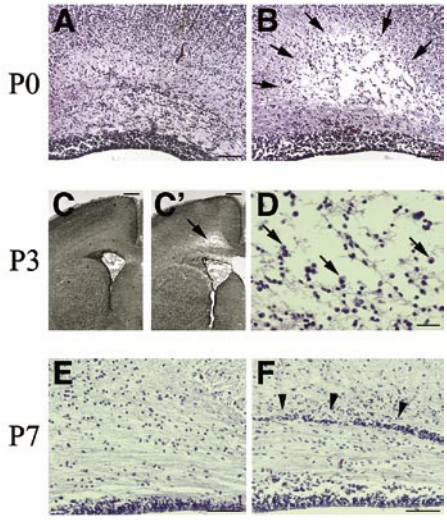

Figure 2. *Hematein-eosin stained coronal sections on P0 (***A**, **B***), P3 (***C**, **C'**, **D***) and P7 (***E**, **F***).* **A**, **C**, **E**: control groups. **B**, **C'**, **D**, **F**: hypoxic groups. Note cystic-like lesions in the white matter delineated by arrows on P0 in **B** and on P3 in **C'**. Enlarged view of this area in **C'** infiltrated by several macrophages (arrows in **D**). Glial scars shown by arrowheads on P7 (F). Bar = 20 µm (**D**); 40 µm (**A**, **B**, **E-F**); 100 µm (**C**, **C'**).

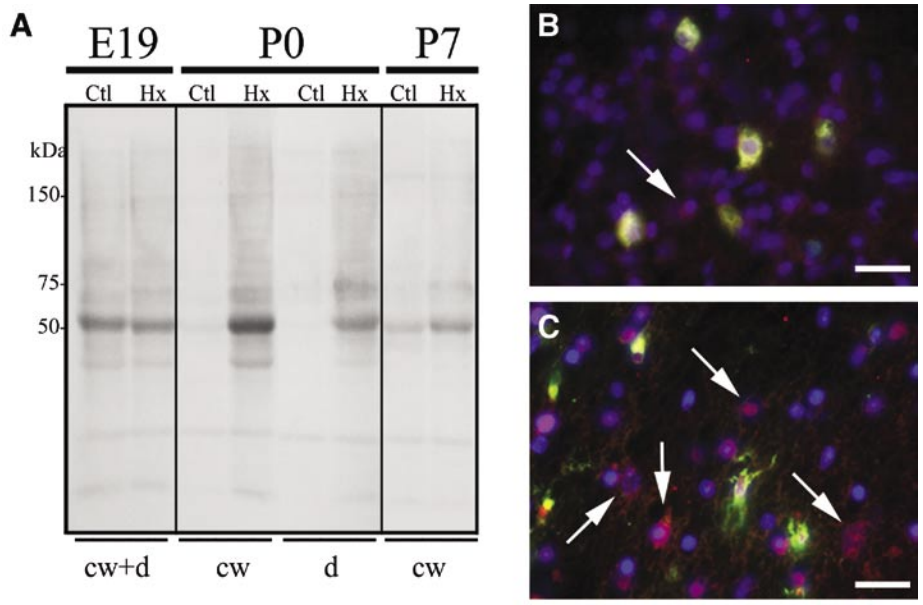

Figure 3. A. Western blot analysis of HNE-coupled proteins (Michael adducts) in the cerebral wall: (cw) and ventral prosencephalon (d: diencephalon and basal ganglia) of control (Ctl) and hypoxic groups (Hx) on E19, P0, and P7. Quantitative analysis was performed by comparing the 50 kDa band between the control group and hypoxic group using Quantity One software (Biorad). **B**, **C**. Triple fluorescent labeling of control (**B**) and hypoxic (**C**) cingular white matter on P0. Note the more numerous HNE positive cell bodies in red (arrows) in **C** compared to **B**.
Macrophages and microglial cells are labeled in green by tomato lectin and their nuclei in blue by DAPI. Bar = 20 µm.

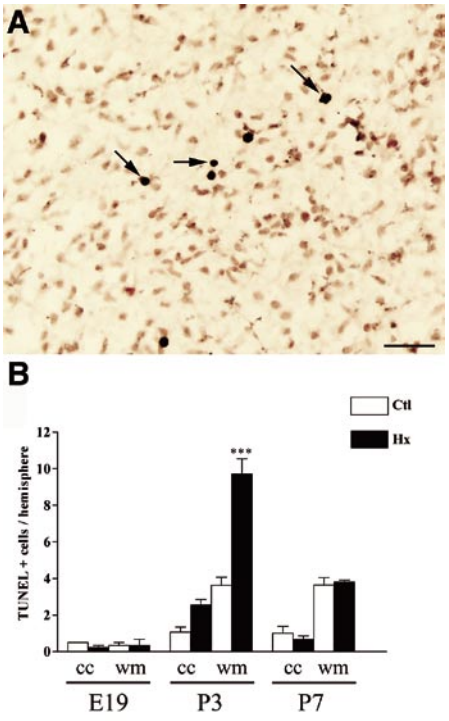

Figure 4. **A.** Coronal sections with TUNEL staining in cingular white matter on P3 in a hypoxic pup. Several labeled nuclei are indicated by arrows. Bar = 10 µm. **B.** Quantitative analysis of TUNEL+ cell density in the subcortical white matter (wm) and corpus callosum (cc). (*** p<0.001 in ANOVA with the Dunnett multiple comparison test).

warm air circulation system.

Immediately after the last MRI acquisition, the rats were decapitated and the brains removed and fixed in formalin for histological studies. After paraffin embedding, coronal 10-µm thick sections were stained with hematein-eosin or Nissl stain or immunostained for GFAP and tomato lectine.

Signal measurements. T2 and T1 sequences. White matter (WM) signal intensity (SI) in the cingulum and external capsule were scored as follows: grade 1 if WM SI was greater than CSF SI on T1 images and less than CSF SI on T2 images; or grade 2 if WM SI was equal to CSF SI on T1 and T2 images.

Apparent diffusion coefficient (ADC) maps and diffusion measurements. The apparent diffusion coefficient (ADC) provides a measure of random water diffusion within tissue and varies with overall water content and tissue composition and organization (9, 30). Therefore, quantitative assessment of brain water ADC by diffusion MR imaging provides the capability to measure in vivo changes in the developing white matter in human and animal newborns. ADC was calculated, pixel by pixel, according to the equation $S(b) = S(0).\exp(-b.ADC)$ where S(b) is the signal intensity at a given b value and S(0) is the signal intensity without a diffusion gradient (b0). To achieve ADC maps, a nonlinear least-squares fit was implemented in each direction. Regions of interest (ROI) were placed on b0 images (no diffusion gradient) and were transferred to ADC maps to extract corresponding ADC values. ADC values were measured in the cingulum and external capsule and compared between normoxic and hypoxic pups.

Statistical analysis. All data are reported as mean ± SEM. Differences between hypoxic and normoxic ADC values were evaluated using the nonparametric Mann-Whitney test. MRI scans were read and ADC measured by 2 investigators (JLD, GS) who were blinded to group assignment.

RESULTS

Prenatal hypoxia induced intra-uterine growth retardation. No difference in body temperature was found at rest between the hypoxic and control groups at any of the developmental stages studied. As previously reported, about 12% of the dams subjected to hypoxia had resorption of all their fetuses and the remaining dams had 40 to 50% smaller litters than did the control dams. Prenatal hypoxia was associated with significant reductions in body weights of the pups on P0 (17%, P<0.001), P3 (10%, P<0.05), P7 (15%, P<0.001), and P14 (28%, P<0.001) but not on P21. In contrast, no differences were found between the hypoxic and control dams for serum lactate, pyruvate, or ketone bodies on day 19 of gestation (Table 2).

Prenatal hypoxia enhanced perinatal angiogenesis in brain parenchyma. GLUT1-immunoreactivity visualized the vessel walls on coronal sections. Vessel wall density was evaluated in the cortical plate and white matter (cingulum) at the level of the septum (Figures 18 to 20 in Paxinos atlas [22]) (Figure 1A, B). From E19 to P3, vessel wall density at both sites was 30% to 40% greater in the hypoxic pups as compared to control pups (Figure 1C). A smaller difference was found on P7 and normalization was noted on P14.

Prenatal hypoxia was associated with specific white matter lesions. Hematoxylin-eosin staining (H&E) of sections from hypoxic animals did not reveal any lesions or spontaneous bleeding in the cortical plate. White matter of E19 fetuses displayed a similar aspect in the normoxic and hypoxic groups. In contrast, focal lesions were observed in the white matter of most of the hypoxic animals killed on P0 (Figure 2A, B) (79%, n = 14), P3 (Figure 2C, 2C′ and 2D) (94%, n = 17) and, to a lesser extent, P7 (20%, n = 15) (Table 3). On P0 and P3, the white matter displayed a "moth-eaten" aspect with cystic-like lesions, as well as more numerous macrophages (Figure 2D) and decreased cell density, predominating in the cingulum (Figure 2A-D) but present also in the external capsule.

On P7, only 20% of the brains displayed similar cystic-like lesions; most of the brains (80%) had no cysts, but instead exhibited a densely populated white matter with several glial scars (Figure 2E, F). Finally, on P14, all hypoxic pups displayed a densely populated white matter with severe gliosis. No bleeding was seen in the white matter at any of the developmental stages studied.

Pup reoxygenation was associated with neonatal oxidative stress. Increased lipid peroxidation in the white matter of hypoxic pups was shown as an increase in reduced 4-Hydroxy-2-Nonenal (HNE), detected using Western blot (Figure 3A) or immunocytochemistry at P0 (Figure 3B, C). Western blot showed that this increase occurred immediately after birth and during the first week of life but was not present at E19 and involved the cerebral wall and the ventral telencephalon-diencephalon (Figure 3A). In the cerebral wall, a 7-fold increase in major HNE-modified proteins was shown on P0 in hypoxic pups as compared to the controls. A residual 1.7-fold increase was noted on P7.

Prenatal hypoxia was associated with increased cell death in white matter. When compared to controls, brains from hypoxic pups showed a significantly increased number of TUNEL-positive nuclei in the white matter underlying the cerebral cortex on P3 (Figure 4A, B). This difference was observed predominantly in the cingular white matter. A similar trend was observed in the corpus callosum, although the difference between the 2 groups was not statistically significant. On E19-P0 and P7, TUNEL staining of the same area was similar in the 2 groups.

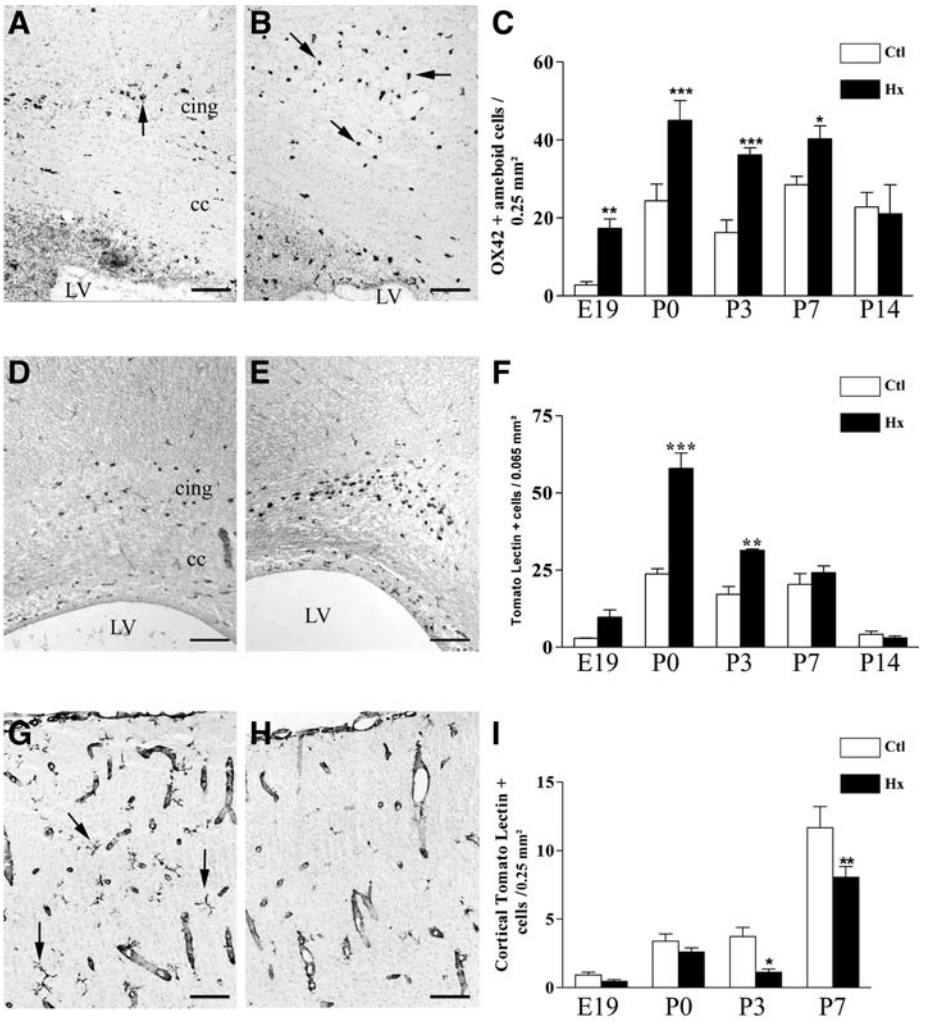

Figure 5. Coronal sections from control (**A**, **D**, **G**) and hypoxic pups (**B**, **E**, **H**) on P3. Immunolabeling for OX42 (**A**, **B**) (arrows indicate activated macrophages in the cingulum (cing) and corpus callosum [cc]). Tomato lectin labeling was performed on paraffin-embedded (**D**, **E**) and frozen sections (**G**, **H**). Arrows indicate resting microglia prominent in the control cortex (**G**). LV: lateral ventricle. Bar = 40 µM. Quantitative analysis of OX42 plus cells in white matter (**C**) and tomato lectin positive cells (activated microglia) in white matter (**F**) and cortical plate (resting microglia) (**I**) according to age. (***p<0.001, **p<0.01, *p<0.05, in 2-way ANOVA with the Bonferroni comparison post test).

Prenatal hypoxia was associated with an inflammatory response in the white matter. Labeling with OX42 and *Lycopersicon esculentum* (tomato) lectin visualized resident and activated microglial cells according to their morphological features (18). During the first week of life in the control pups, ameboid/activated microglial cells were detected in the cingulum, internal and external capsules, periventricular area, and germinal matrix, but not in the cortical plate. The spatial-temporal distribution of the microglia was not altered in hypoxic pups, but the microglial cell counts were higher than in the controls. A greater than 2-fold increase in activated macrophages labeled with OX42 (Figure 5A-C) and tomato lectin (Figure 5D-F) was found in hypoxic brains as compared to normoxic brains during the perinatal period, the difference being statistically significant on P0 and P3. This inflammatory response was still present in about 20% of brains on P7. Conversely, the resident microglial cells, which were well visualized by tomato lectin labeling, were less numerous in the cortical layers of the hypoxic than normoxic animals (Figure 5G-I).

Extracellular matrix was modified in the periventricular white matter of hypoxic pups. To further analyze the white matter lesions shown in the hypoxic brains by

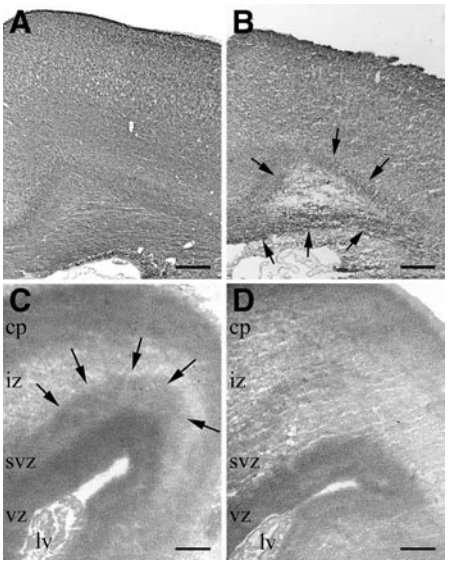

Figure 6. Frontal sections with PSA-NCAM immunostaining in pups on P3 under control (**A**) or hypoxic conditions (**B**). Note the labeling in the white matter around the cystic-like lesion delineated by arrows; Bar = 60 µm.
Coronal sections showing in situ hybridization for aggregan gene transcripts (exons 4-10) in the cerebral wall at E19 in control (**C**) and hypoxic group (**D**). Arrows indicated aggrecan gene transcription in the subventricular zone (svz) in C. cp: cortical plate; iz: intermediate zone; vz: ventricular zone; lv: lateral ventricle.

H&E (Figure 2), PSA-NCAM staining was performed on adjacent sections. On P0 and P3, PSA-NCAM immunoreactivity was increased around the white matter lesions in the hypoxic animals as compared to the normoxic animals (Figure 6A, B). No difference was detected at the older stages.

On E19, a decrease in aggrecan gene transcripts related to extracellular matrix maturation was noted in the hypoxic brains. In situ hybridization with aggrecan gene probes for exons 4 to 10, or exon 12, demonstrated strong labeling of the white matter in the subventricular zone of the control pups but not of the hypoxic pups at the same developmental stage (Figure 6C and 6D). In contrast, no difference was observed using the TGF-β2 probe. Similar experiments on P3 and P7 did not show any difference between the 2 groups with any of the probes.

Astrogliosis was associated with white matter lesions. Several glial scars were revealed by H&E in the white matter of hypoxic pups but not of normoxic pups. They were first observed in a few hypoxic pups on P3 and were more marked on P7 in the cingulum (Figure 2E, F) and, to a lesser extent, in the postero-lateral part of the external capsule.

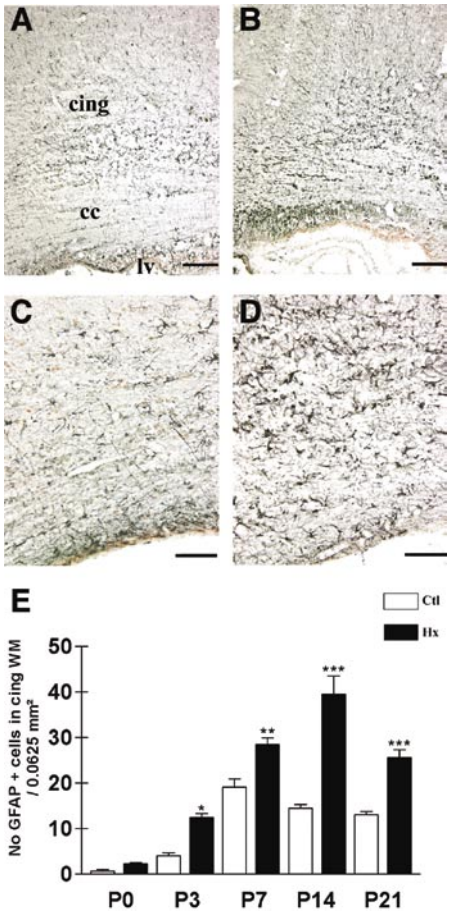

Figure 7. Coronal sections showing GFAP immunostainings on P7 (**A**, **B**) and P14 (**C**, **D**) in controls (**A**, **C**) and hypoxic pups (**B**, **D**).
cing: cingulum, cc: corpus callosum, lv: lateral ventricle. Bar = 30 µm.
Quantitative analysis of GFAP-positive cells from P0 to P21 (**E**). (***p<0.001, ** p<0.01, *p<0.05 in 2-way ANOVA with the Bonferroni comparison post test).

To analyze cell types in the glial scars, labeling with both anti-S100 β protein (data not shown) and anti-GFAP (Figure 7A-D) was performed. Mature GFAP-positive astrocytes were scattered in the white matter as early as P3 in the hypoxic brains. Reactive astrocytes counts were significantly higher in the white matter of hypoxic pups compared to those of normoxic pups from P3 to P21 (Figure 7E). Mature astrocytes displayed an activated aspect with an increased number of processes and larger cell bodies in the hypoxic brains (Figure 7D).

Myelination was impaired after white matter damage. Markers for immature oligodendocytes (O4) and mature oligodendrocytes (MBP) were used on P7 and P14 to compare the myelination process in hypoxic and normoxic brains. The quantitative analysis of coronal sections at the same level as above showed a 2-fold decrease in the number of O4-positive preoligodendrocytes in the white matter on P7 (Figure 8A-C). Similarly, anti-MBP staining revealed a 3-fold decrease in the number of myelin fascicles in both the corpus callosum and the cingular white matter on P7 (Figure 8D-F). This delay in myelination was still seen on P14 as a decrease in the thickness of the fascicles of myelinated axons in the telencephalon (Figure 8G, H). It involved not only the cortical white matter but also the fascicles in the basal ganglia, internal capsule, and thalamus. Impaired myelination was strongly associated with the presence of glial scars in the cingulum (Figure 8I, J). Slight but non significant differences were still observed between the 2 groups on P21 (Figure 8K, L). This delay in the myelination process in hypoxic brains during the first 2 postnatal weeks was not related to a decreased number of axons labeled by the neurofilament marker RT97: no difference in the pattern of distribution of this axonal marker was observed in hypoxic compared to control brains.

White matter lesions were detected using in vivo magnetic resonance imaging. On P0, all cases scored grade 2 (see Methods) were hypoxic animals and all cases scored grade 1 were normoxic animals. The mean ADC values in grade 1 pups (ie, normoxic pups) were $0.92 \pm 0.05 \times 10^{-3}$ mm²/s in the cingulum and $0.90 \pm 0.05 \times 10^{-3}$ mm²/s in the lateral external capsule. ADC was significantly greater for animals scored grade 2 (hypoxic pups): $1.30 \pm 0.01 \times 10^{-3}$ mm²/s in the cingulum ($p<0.01$) and $1.26 \pm 0.02 \times 10^{-3}$ mm²/s in the lateral external capsule ($p<0.05$) (Figure 9A, G). This difference, with no overlap, reflected a 42% increase in ADC correlated with the inflammatory features shown by tomato lectin staining in the same structures (Figure 9C, D, G, H). A diffusion threshold, equal to $1.20 \pm 0.03 \times 10^{-3}$ mm²/s, discriminated all hypoxic pups from control pups.

In contrast, on P7, T2 and T1 images failed to discriminate between hypoxic and normoxic pups. The diffusion study showed that grade 1 cases fell into 2 groups based on ADC values. In one group, mean ADC was $1.25 \pm 0.04 \times 10^{-3}$ mm²/s in the cingu-

lum and $1.19 \pm 0.02 \times 10^{-3}$ mm^2/s in the external capsule (Figure 9B, G). All pups in this group were controls. Mean ADC value was significantly lower in the other group: $1.00 \pm 0.03 \times 10^{-3}$ mm^2/s in the cingulum ($p<0.01$) and $1.07 \pm 0.02 \times 10^{-3}$ mm^2/s in the external capsule ($p<0.01$). These lower values correlated with prenatal hypoxia. This difference, corresponding to a 20% and 11% decrease in the cingulum and external capsule, respectively, was associated with the presence of many GFAP-positive astrocytes and higher cellular density (Figure 9E-G).

Three additional hypoxic animals were scored grade 2. Diffusion maps showed large regions where ADC values were significantly increased compared to the control pups. In all 3 cases, a persistent inflammatory process was visible in both the cingulum and the external capsule, with a significant increase in activated macrophages as compared to normoxic animals and to most hypoxic animals on P7.

DISCUSSION

The present study describes a new model of perinatal white matter damage following protracted prenatal hypoxia. Early events included focal white matter microglial activation and increased lipid peroxidation indicating a local inflammatory response and oxidative stress. Focal white matter lesions were associated with secondary astrogliosis and abnormal myelination. These lesions were found using several techniques, including standard histological procedures in both paraffin-embedded and frozen sections, immunohistochemistry, western blotting, in situ hybridization for extracellular matrix-related genes, and in vivo MRI.

In this model, prenatally occurring hypoxemia was confirmed by several findings: restricted growth, as reported in previous studies (4, 7, 16, 33); increased vessel wall density in several brain areas consistent with a transient adaptive response to fetal hypoxemia; and an increase in hypoxia-inducible factor-1 mRNA, a transcription factor activated only by cellular hypoxia, in keeping with earlier findings (26). One possible effect of protracted hypoxia during gestation may be nonspecific stress to the dam, which might in turn affect the fetuses. However, the pregnant dams subjected to hypoxia showed no behavioral evidence of stress and had similar corticosterone levels to those in the control rats (16). In contrast, plasma adrenaline and noradrenaline levels were markedly increased in the pregnant dams subjected to hypoxia, as compared to the pregnant controls. However, most maternal catecholamines are inactivated by the placenta making unlikely the possibility of a catecholamine-induced reduction in umbilical flow.

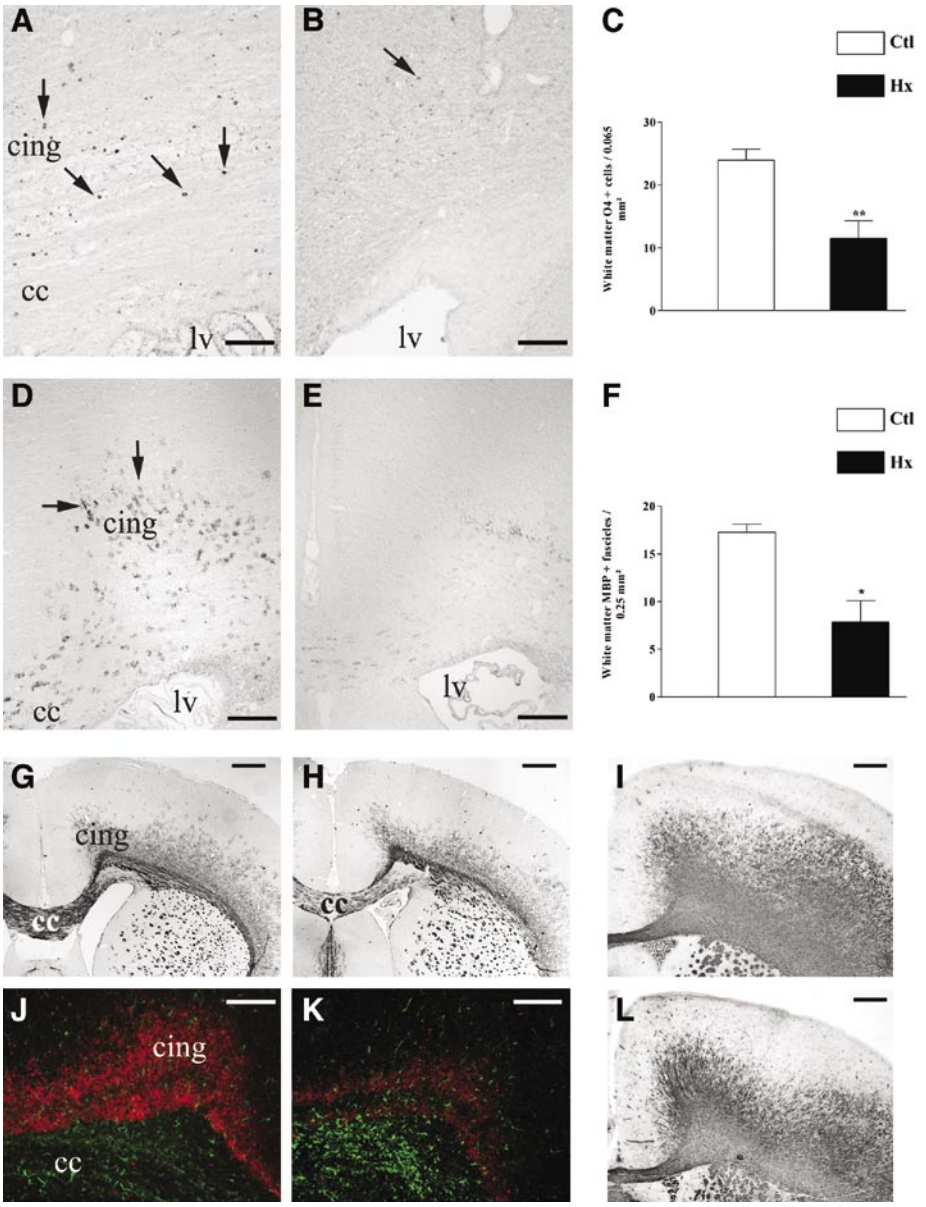

Figure 8. Coronal sections immunolabeled with O4 (**A**, **B**) (arrows indicated labeled preoligodendrocytes) or MBP (**D**, **E**, **G**, **H**, **I**, **L**) immunostainings on P7 (**A**, **B, D, E**), P14 (**G**, **H, I, K**) and P21 (**I**, **L**) in pups under control (**A**, **D**, **G**, **I, J**) and hypoxic conditions (**B**, **E**, **H**, **K, L**). Note the larger number of MBP-positive axon fascicles in **D** (arrows) than in **E** and the delayed myelination in the cingulum (cing) and corpus callosum (cc) (**G**, **H**).

Quantitative analysis of O4-positive cell density (**C**) and MBP-positive fascicle density (**F**) in the white matter. (** $p<0.01$, * $p<0.05$ by the Mann-Whitney test).

Double immunolabeling of coronal sections using anti-O4 (red) and anti-GFAP (green) antibodies in the control group (**J**) and hypoxic group (**K**) in white matter on P14. Note the reactive GFAP-positive astrocytes contiguous to strong O4 labeling in the cingulum. cing: cingulum, cc: corpus callosum. Bar = 30 µm (**A**, **B**, **D**, **E**), 100 µm (**G, H, I, L**), 40 µm (**J, K**).

Despite several technical limitations, we cannot rule out the contribution of ischemia to the focal lesions observed. This issue is of particular importance as cerebral ischemia/reperfusion has been thought to be a major risk factor in the genesis of human PVL through the combination of excitotoxicity and oxidative/nitrosative stress (6, 8). However, the main features detected in the clinical, biochemical and

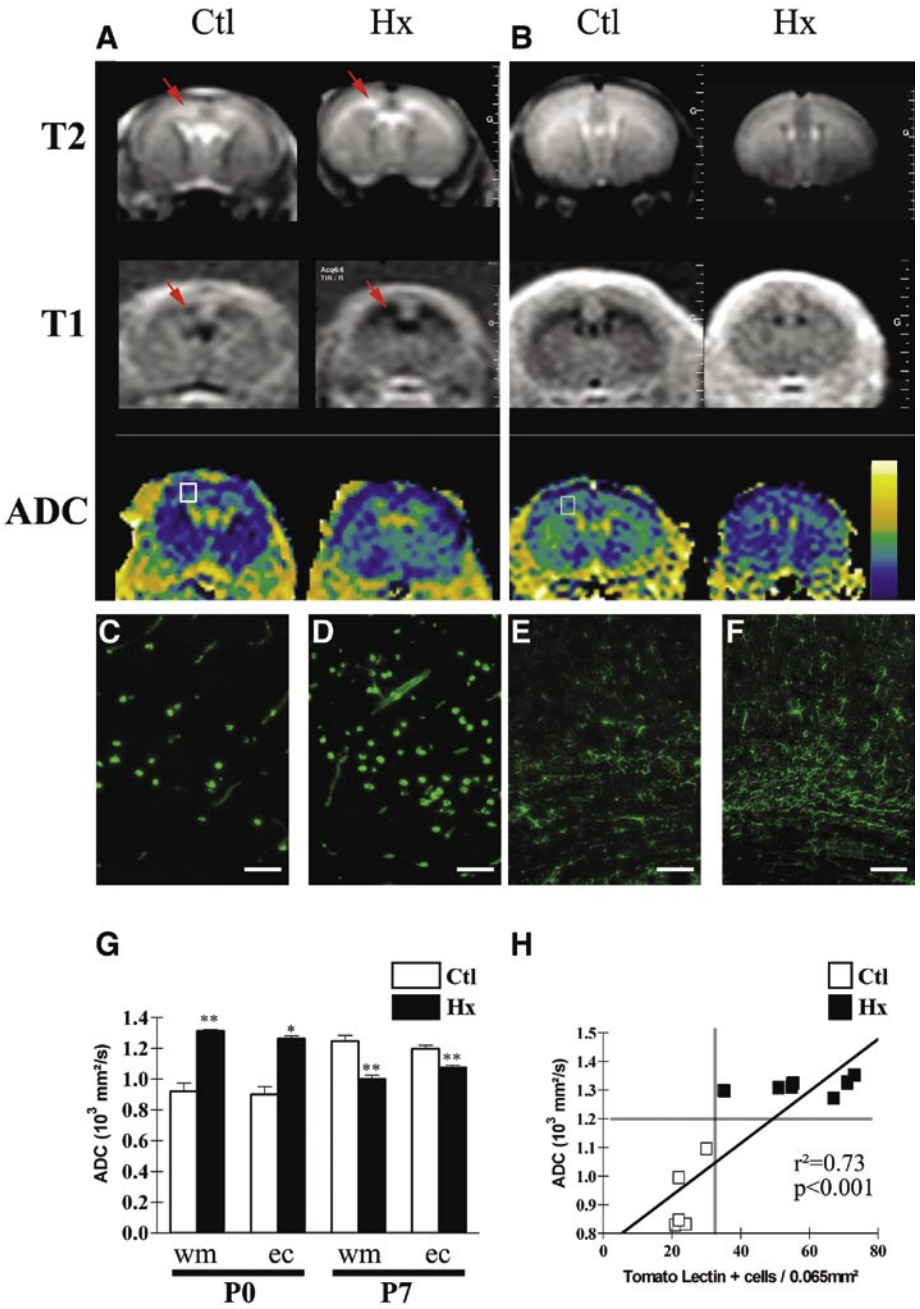

Figure 9. In vivo MRI assessment of white matter lesions and histological correlations. T2, T1, and diffusion sequences performed either on P0 (**A**) or on P7 (**B**) pups. Red arrows indicate the cingular white matter. White frames on ADC maps correspond to:
(i) Area of the coronal section immunostained either with tomato lectin antibodies (activated microglia) on P0 in control (**C**) or hypoxic (**D**) pups or with GFAP antibodies (reactive astrocytes) on P7 in control (**E**) or hypoxic (**F**) pups. Bar = 30 µm.
(ii) Region of interest for ADC measurements.
G. Quantitative analysis of ADC values in cingular white matter (wm) and external capsule (ec). (** $p<0.01$, * $p<0.05$ in Mann-Whitney test).
H. Linear regression between ADC values and tomato lectin-positive cell density in the cingular white matter.

histochemical analyses of our rat model appear to be closer to hypoxia than to global ischemia. Nevertheless, the causal factor inducing the white matter damage described here remains to be elucidated. Another crucial question is which rat age could best coincide with the human age for the peak time of PVL. According to previous reports, the periventricular germinal matrix composition and global brain development in the rat brain on P6 are roughly similar to the developmental stage of the human brain at 38 to 40 weeks of postconceptional age (5, 34). The rat pup brain at birth (P0) is likely to correspond to the human brain around 22 to 24 weeks of gestation. Therefore, in our model the trigger of the cerebral white matter damage could occur at a developmental stage corresponding to the extreme prematurity observed in human (22-26 weeks gestation). This is of particular clinical relevance as a growing number of neonates survive from extremely premature delivery and subsequently develop neurological impairment.

Our main findings are that prenatal hypoxia was associated with local inflammation and oxidative stress in the pup brains with the development of white matter cysts and a delay in myelination. To understand the pathophysiologic process involved in white matter damage, determining the timing and interrelations of these events is crucial (Figure 10). Severe oxidative stress was detected in the brains of the hypoxic pups at birth, using reduced-HNE staining and immunoblotting. HNE is the major aldehyde generated by free radical attack and is largely responsible for the damage associated with oxidative stress (38). Microglial activation in the white matter seems to have occurred a bit later, with a peak on P3. It was located in the same white matter areas as the transient and milder microglial activation seen in the normal pups with a peak on P8. Microglial activation may contribute to normal remodeling following physiological developmental apoptosis (18). The microglial activation in the hypoxic pups might have been a response either to the protracted prenatal hypoxia or to the combination of prenatal hypoxia and reoxygenation starting on the day before birth. The evidence of oxidative stress found by HNE staining and immunoblot at birth supports the second possibility. Microglial activation occurred in close association with white matter cell death and cyst formation and preceded the occurrence of defective myelination. Several studies found that immature oligodendrocytes were highly vulnerable to oxidative stress in vitro or in vivo, especially in the presence of activated macrophages (15). In our model, one hypothesis is a primary role for local microglial cell activation in the genesis of the white matter lesions, with the activation being a response to oxidative stress and reoxygenation-associated abnormalities,

and the marked vulnerability of immature oligodendrocytes to these insults leading to defective myelination (Figure 10).

The extent to which the combination of cell dysfunctions shown in our new model of white matter damage (table 3) mimic the pathological processes underlying periventricular leukomalacia in humans and present in other models for PVL deserves careful discussion.

i. We found evidence of an increased inflammatory response in the white matter. This finding is congruent with epidemiological and experimental studies indicating that intrauterine infection and chorioamnionitis can contribute to the pathogenesis of PVL (36, 37). However, published evidence that inflammation contributes to the pathogenesis of PVL was obtained in situations combining hypoxia/ischemia and infection (8). Lipopolysaccharide and similar bacterial elements have been shown to damage oligodendrocytes and myelin through a specific receptor for several microbial molecular motifs present on the microglial membrane (15). Evidence for a central role for the microglia has been obtained also in another excitotoxic model of murine PVL (28).

ii. The increased number of TUNEL+ cells in the brains from hypoxic pups in our study suggests increased cell death in the white matter on P3. This finding may be relevant to the decreased number of preoligodendrocytes on P7, which was associated with impaired myelination involving mature oligodendrocytes (MBP-immunoreactivity). The intrinsic vulnerability of preoligodendrocytes is considered central to the pathogenesis of PVL (32). Several reports suggest that immature oligodendrocytes may be more vulnerable than mature oligodendrocytes to oxidative stress caused by either hypoxic-ischemic insults in vivo or depletion of intracellular glutathione in vitro (1, 2, 6). Our model showed a 2-fold decrease in O4+ preoligodendrocytes in the hypoxic brain on P7. This inadequacy of the oligodendrocyte pool to ensure normal myelination might be an accurate short-term tool for testing the ability of several neuroprotective treatments to prevent white matter damage in this model.

iii. Astrogliosis was found consistently in our model. Reactive astrocytes are a typical feature of PVL in humans (21). Our finding that some reactive astrocytes expressed the O4 marker suggests that glial activation may have been related to an inflammatory process, as recently reported in an interferon-induced inflammation model (13).

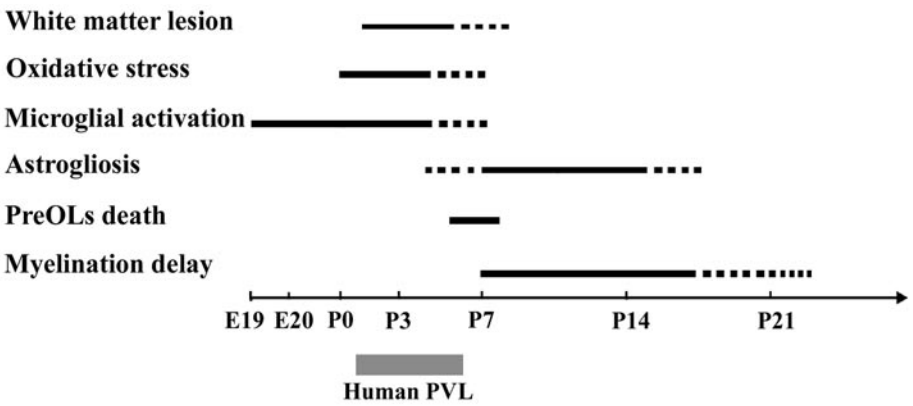

Figure 10. Timing of the main events observed in the white matter of rat fetuses/pups subjected to protracted gestational hypoxia. White matter lesion is defined by the presence of cystic-like destruction of the cingular white matter on at least 500 µm in the anterio-posterior axis. Line and dotted line mean, respectively, a significant and a non significant difference for each parameter between rat pups born from hypoxic mother as compared to control.

iv. In vivo MRI findings obtained using T1, T2, and diffusion sequences were abnormal immediately after birth. The apparent diffusion coefficient (ADC) provides a measure of random water diffusion within tissues and varies with overall water content and tissue composition and organization (9, 30). Therefore, diffusion MRI can be used for the in vivo measurement of developmental microstructural changes in the white matter, including changes in fiber size and orientation (10, 19, 25, 35). We found striking differences in white-matter ADC between the hypoxic and control groups, in accordance with our histological findings. These ADC changes were particularly interesting on P7, when no differences were found for T1 and T2 images between the hypoxic and control groups (24, 30). These observations suggest that MRI may be a powerful tool for defining and monitoring hypoxia-induced white matter injury in newborns.

Further studies are needed to correlate neuropathological lesions, imaging findings and neurological deficits in this model. Modifications in the circadian rhythm of locomotor activity of rat born from hypoxic pregnant rats was already partly reported (11).

In conclusion, the present model mimics most of the commonly observed features of white matter damage observed in preterm human neonates. Among previously described animal models, most are based on an acute external injury such as an intracerebral injection or an ischemic surgical procedure. Our noninvasive model may prove valuable for unraveling the sequence of events that lead to PVL. One must keep in mind, however, that human PVL is an extremely complex multifactorial disorder that must be investigated via a variety of in vitro and in vivo approaches.

REFERENCES

1. Back SA, Gan X, Li Y, Rosenberg PA, Volpe JJ (1998) Maturation-dependent vulnerability of oligodendrocytes to oxidative stress-induced death caused by glutathione depletion. *J Neurosci* 18:6241-6253.

2. Back SA, Han BH, Luo NL, Chricton CA, Xanthoudakis S, Tam J, Arvin KL, Holtzman DM (2002) Selective vulnerability of late oligodendrocyte progenitors to hypoxia-ischemia. *J Neurosci* 22: 455-463.

3. Baud O, Fayol L, Gressens P, Pellerin L, Magistretti P, Evrard P, Verney C (2003) Perinatal and early postnatal changes in the expression of monocarboxylate transporters MCT1 and MCT2 in the rat forebrain. *J Comp Neurol* 465:445-454.

4. de Grauw TJ, Myers RE, Scott WJ (1986) Fetal growth retardation in rats from different levels of hypoxia. *Biol Neonate* 49:85-89.

5. Dobbing J (1974) The later development of the brain and its vulnerability. In: *Scientific Foundation of Paediatrics*, edited by Davis JA and Dobbing J. London: Heinemann, p565-77.

6. Follett PL, Rosenberg PA, Volpe JJ, Jensen FE (2000) NBQX attenuates excitotoxic injury in developing white matter. *J Neurosci* 20:9235-9241.

7. Gleed RD, Mortola JP (1991) Ventilation in newborn rats after gestation at simulated high altitude. *J Appl Physiol* 70:1146-1151.

8. Hagberg H, Peebles D, Mallard C (2002) Models of white matter injury: comparison of infectious,

hypoxic-ischemic, and excitotoxic insults. *Ment Retard Dev Disabil Res Rev* 8:30-38.

9. Hoehn M, Nicolay K, Franke C, van der Sanden B (2001) Application of magnetic resonance to animal models of cerebral ischemia. *J Magn Reson Imaging* 14:491-509.

10. Huppi PS, Maier SE, Peled S, Zientara GP, Barnes PD, Jolesz FA, Volpe JJ (1998) Microstructural development of human newborn cerebral white matter assessed in vivo by diffusion tensor magnetic resonance imaging. *Pediatr Res* 44: 584-590.

11. Joseph V, Mamet J, Lee F, Dalmaz Y, Van Reeth O (2002) Prenatal hypoxia impairs circadian synchronisation and response of the biological clock to light in adult rats. *J Physiol* 543:387-395.

12. Kok JH, den Ouden AL, Verloove-Vanhorick SP, Brand R (1998) Outcome of very preterm small for gestational age infants: the first nine years of life. *Br J Obstet Gynaecol* 105:162-168.

13. Kong GY, Kristensson K, Bentivoglio M (2002) Reaction of mouse brain oligodendrocytes and their precursors, astrocytes and microglia, to proinflammatory mediators circulating in the cerebrospinal fluid. *Glia* 37:191-205.

14. Kuban KC, Leviton A (1994) Cerebral palsy. *N Engl J Med* 330:188-195.

15. Lehnardt S, Lachance C, Patrizi S, Lefebvre S, Follett PL, Jensen FE, Rosenberg PA, Volpe JJ, Vartanian T (2002) The toll-like receptor TLR4 is necessary for lipopolysaccharide-induced oligodendrocyte injury in the CNS. *J Neurosci* 22: 2478-2486.

16. Mamet J, Peyronnet J, Roux JC, Perrin D, Cottet-Emard JM, Pequignot JM, Lagercrantz H, Dalmaz Y (2002) Long-term prenatal hypoxia alters maturation of adrenal medulla in rat. *Pediatr Res* 51:207-214.

17. Marret S, Gressens P, Evrard P (1996) Arrest of neuronal migration by excitatory amino acids in hamster developing brain. *Proc Natl Acad Sci U S A* 93:15463-15468.

18. Milligan CE, Cunningham TJ, Levitt P (1991) Differential immunochemical markers reveal the normal distribution of brain macrophages and microglia in the developing rat brain. *J Comp Neurol* 314:125-135.

19. Neil JJ, Shiran SI, McKinstry RC, Schefft GL, Snyder AZ, Almli CR, Akbudak E, Aronovitz JA, Miller JP, Lee BC, Conturo TE (1998) Normal brain in human newborns: apparent diffusion coefficient and diffusion anisotropy measured by using diffusion tensor MR imaging. *Radiology* 209:57-66.

20. Nyakas C, Buwalda B, Luiten PG (1996) Hypoxia and brain development. *Progress in Neurobiology* 49:1-51.

21. Okoshi Y, Itoh M and Takashima S (2001) Characteristic neuropathology and plasticity in periventricular leukomalacia. *Pediatr Neurol* 25: 221-226.

22. Paxinos G, Watson C (1998) *The rat brain in stereotaxic coordinates, fourth edition.* Academic press, San Diego, CA, USA.

23. Peyronnet J, Roux JC, Geloen A, Tang LQ, Pequignot JM, Lagercrantz H, Dalmaz Y (2000) Prenatal hypoxia impairs the postnatal development of neural and functional chemoafferent pathway in rat. *J Physiol* 524:525-537.

24. Qiao M, Malisza KL, Del Bigio MR, Tuor UI (2002) Transient hypoxia-ischemia in rats: changes in diffusion-sensitive MR imaging findings, extracellular space, and Na+-K+ -adenosine triphosphatase and cytochrome oxidase activity. *Radiology* 223:65-75.

25. Robertson RL, Ben-Sira L, Barnes PD, Mulkern RV, Robson CD, Maier SE, Rivkin MJ, du Plessis A (1999) MR line-scan diffusion-weighted imaging of term neonates with perinatal brain ischemia. *AJNR Am J Neuroradiol* 20:1658-1670.

26. Royer C, Lachuer J, Crouzoulon G, Roux J, Peyronnet J, Mamet J, Pequignot J, Dalmaz Y (2000) Effects of gestational hypoxia on mRNA levels of Glut3 and Glut4 transporters, hypoxia inducible factor-1 and thyroid hormone receptors in developing rat brain. *Brain Res* 856:119-128.

27. Schwartz NB, Domowicz M, Krueger RC, Jr., Li H, Mangoura D (1996) Brain aggrecan. *Perspect Dev Neurobiol* 3:291-306.

28. Tahraoui SL, Marret S, Bodenant C, Leroux P, Dommergues MA, Evrard P, Gressens P (2001) Central role of microglia in neonatal excitotoxic lesions of the murine periventricular white matter. *Brain Pathol* 11:56-71.

29. Vassault A, Bonnefont JP, Specola N, Saudubray JM (1991) Lactate, pyruvate and ketone bodies. In: *Techniques in diagnostic human biochemical genetics. A laboratory manual.* Homme FA (ed), pp 285-308, Wiley-Liss: New York.

30. Verheul HB, Balazs R, Berkelbach van der Sprenkel JW, Tulleken CA, Nicolay K, Tamminga KS, van Lookeren Campagne M (1994) Comparison of diffusion-weighted MRI with changes in cell volume in a rat model of brain injury. *NMR Biomed* 7:96-100.

31. Verney C, Takahashi T, Bhide PG, Nowakowski RS, Caviness VS, Jr (2000) Independent controls for neocortical neuron production and histogenetic cell death. *Dev Neurosci* 22:125-138.

32. Volpe JJ (2001) Neurobiology of periventricular leukomalacia in the premature infant. *Pediatr Res* 50:553-562.

33. White LD, Lawson EE (1997) Effects of chronic prenatal hypoxia on tyrosine hydroxylase and phenylethanolamine-N-methyltransferase messenger RNA and protein levels in medulla oblongata of postnatal rat. *Pediatr Res* 42: 455-462.

34. Whitelaw A, Thoresen M (2000) Antenatal steroids and the developing brain. *Arch Dis Child Fetal Ed* 83:F154-7.

35. Wolf RL, Zimmerman RA, Clancy R, Haselgrove JH (2001) Quantitative apparent diffusion coefficient measurements in term neonates for early detection of hypoxic-ischemic brain injury: initial experience. *Radiology* 218:825-833.

36. Wu YW, Colford JM, Jr (2000) Chorioamnionitis as a risk factor for cerebral palsy: A meta-analysis. *JAMA* 284:1417-1424.

37. Yoon BH, Jun JK, Romero R, Park KH, Gomez R, Choi JH, Kim IO (1997) Amniotic fluid inflammatory cytokines (interleukin-6, interleukin-1beta, and tumor necrosis factor-alpha), neonatal brain white matter lesions, and cerebral palsy. *Am J Obstet Gynecol* 177:19-26.

38. Zarkovic N (2003) 4-Hydroxynonenal as a bioactive marker of pathological processes. *Mol Aspects Med* 24:281-291.